Research Article Vol. 30, No. 1 / 3 Jan 2022 / Optics Express 619
Optics EXPRESS

Simplified twin-single-sideband direct detection system separating left and right sideband signals using a digital signal processing algorithm instead of optical bandpass filters

YE ZHOU,[1] JIANGNAN XIAO,[1,*] CHUANG ZHAO,[1] JIANGLI ZUO,[1] JUN MING,[1] AND LI ZHAO[2]

[1] University of Shanghai for Science and Technology, Shanghai 200093, China
[2] School of Information Science and Technology, Fudan University, Shanghai 200433, China
[*] jiangnanxiao@usst.edu.cn

Abstract: Twin-single-sideband (twin-SSB) signals can be generated based on an in-phase–quadrature (I/Q) modulator, and two independent left sideband (LSB) and right sideband (RSB) signals carry individual data to effectively harvest the advantage of twin-SSB modulation, which achieves higher spectral efficiency. However, the conventional twin-SSB scheme employs two optical bandpass filters (OBPFs) and two photodetectors (PDs) for complete separation and detection at the receiver side. To mitigate the crosstalk between RSB and LSB signals and reduce the complexity and cost of the twin-SSB system, we propose a new scheme to realize twin-SSB without OBPFs separating LSB and RSB signals by a single-ended PD to improve system performance. According to the beating characteristics of the LSB and RSB, we can separate two independent sideband signals using a digital signal processing (DSP) algorithm added to the receiver end. Our simulation results demonstrate that our proposed scheme can obtain good bit error ratio (BER) performance of LSB and RSB signals. We designed a twin-SSB system with different modulation formats in the two sidebands, adopting geometric shaping 3PSK (GS-3PSK) modulation for the LSB and quadrature phase shift keying (QPSK) modulation for the RSB. The BER of the LSB GS-3PSK and RSB QPSK signal can reach hard-decision forward error correction (HD-FEC) when the received optical power (ROP) was > -17.5 and > -16 dBm, respectively, at different baud rates of 1-, 2-, and 4-Gbaud with a carrier frequency of 12-GHz over 10-km standard single-mode fiber (SSMF) transmission. For an 8-Gbaud baud rate with a carrier frequency of 12-GHz over 5-km SSMF transmission, the BER of the two sideband signals can still be below the HD-FEC threshold of 3.8×10^{-3} when the ROP was > -17 and > -16 dBm, respectively.

1. Introduction

Currently, owing to the increasing popularity of different mobile broadband applications such as high-quality internet protocol television, cloud computing using remote data storage, virtual reality, and the emergence of a variety of new services such as 5G and live-streaming of high-definition video multimedia, the potential capacity demand imposes challenging burdens on optical fiber transmission systems, which offer high capacity and spectrally efficient signaling with low loss to transmission [1–9]. Future networks are expected to provide simple configurations, high spectral efficiency (SE), and broadband services [10]. A variety of advanced modulation formats have been proposed to improve the spectral efficiency of optical transmission systems, including optical single sideband (O-SSB) [11,12] and optical independent sideband (O-ISB) or twin-SSB schemes [13–16]. O-SSB modulation with direct detection has been proposed for short-distance transmission systems. This is because this scheme not only overcomes the

#446108 https://doi.org/10.1364/OE.446108
Journal © 2022 Received 15 Oct 2021; revised 12 Nov 2021; accepted 21 Nov 2021; published 23 Dec 2021

Optics EXPRESS

power fading induced by chromatic dispersion observed in the transmission of double sideband (DSB) signals but is also capable of doubling the SE by halving the spectral width of DSB signals [17]. In 2013, Sharma [12] proposed a hybrid orthogonal frequency division multiplexing (OFDM) O-SSB radio over fiber system. Improvements of 1.7 and 0.52 dB, respectively, were demonstrated after an optical transmission of 10 and 100 km for the wired hybrid radio over fiber system. In 2020, Lin *et al.* proposed a vector signal generation method based on optical carrier suppression (OCS) and SSB without an OBPF, experimentally demonstrating 2-Gbaud 16-quadrature-amplitude-modulation, 4-Gbaud QPSK, and 10-Gbaud QPSK vector signal generation over 20-km SSMF transmission [18]. One shortcoming of the O-SSB modulation system, however, is that it wastes half the bandwidth of the digital-to-analog converter (DAC) at the transmitter side because it only has one sideband of information. Another shortcoming is that the direct detection of O-SSB suffers from signal-signal beating interference after the PD, and it is essential to sacrifice either the SE by inserting a guard band between the carrier and the SSB signal or the receiver sensitivity by increasing the carrier-to-signal power ratio (CSPR). To fully utilize the DAC bandwidth, the O-ISB or twin-SSB has been proposed [19–22]. Twin-SSB modulation, an efficient modulation technique, evolved from the existing optical DSB and optical SSB modulations**.** Unlike optical DSB, in which one sideband is wasted, twin-SSB makes full use of the two sidebands around a carrier by delivering independent data information over the LSB and the RSB, respectively [23]. In 2018, Deng *et al.* proposed and experimentally demonstrated a heterodyne W-band fiber-wireless system using a twin-SSB orthogonal frequency division multiplexing (twin-SSB-OFDM) transmission system with low-cost electrical filters [24] that can reach a 40.07 Gb/s data rate with a bit error ratio (BER) below the hard-decision forward error correction (HD-FEC) threshold of 3.8×10^{-3} after 22-km SSMF transmission and 1-m wireless transmission. In 2020, Gao *et al.* proposed a zero-guard band multi-twin-SSB bidirectional passive optical network system that combines the multiband carrier-less amplitude phase and twin-SSB modulation techniques [25]. This scheme can efficiently reduce the required optical signal-to-noise ratio (OSNR) and improve receiver sensitivity. All these twin-SSB modulation systems could achieve a higher SE than optical DSB or optical SSB modulation systems. Two steep OBPFs and two PDs were used to separate the LSB and RSB signals. At the receiver side, two sideband signals were processed by two-path DSP. Ideally, OBPFs with rectangular frequency responses can eliminate crosstalk. To the best of our knowledge, almost all existing twin-SSB modulation schemes require two OBPFs and PDs to separate and detect signals at the receiver side. However, part of the residual unwanted sideband signal reduces the system performance because the practical OBPFs normally have a slow roll-off. In addition, the two OBPFs and PDs also improve the system cost and complexity.

In this study, we propose and investigate a novel twin-SSB scheme based on an I/Q modulator. After direct detection by a single-ended PD at the receiver side, we can directly separate the optical LSB and RSB using a simple one-path DSP algorithm without OBPFs separating two sideband signals, thereby achieving lower algorithm complexity and lower complexity and cost of the system while doubling the SE. Using our proposed twin-SSB scheme, we demonstrate 1-, 2-, and 4-Gbaud LSB GS-3PSK and RSB QPSK signal transmission over 10-km of SSMF and an 8-Gbaud rate transmission over 5-km of SSMF. The simulation results demonstrate that the BER of the transmission system is below the HD-FEC threshold of 3.8×10^{-3}.

The remainder of this paper is organized as follows: Section 2 describes the principle of the two-sideband vector signal generation based on the I/Q modulator and theoretical derivations of separating the LSB and RSB signals by DSP. Section 3 presents the DSP algorithms for the system simulation setup. In Section 4, the evaluations of BER performance for LSB GS-3PSK and RSB QPSK signals are provided under different SSMF transmission distances with different baud rates. Finally, the conclusions are summarized in Section 5.

Optics EXPRESS

2. Principle of twin-SSB scheme without OBPFs separating the two sidebands

2.1. Principle of LSB and RSB vector signal generation

Figure 1 shows our scheme to generate two independent LSB and RSB vector signals based on an I/Q modulator. The driving signal I-path and Q-path for the I/Q modulator were generated via DSP. At the transmitter end, two sets of twin-SSB pseudo-random binary sequences (PRBSs) of the same length, denoted as PRBS1 and PRBS2, are individually vector mapped, up-sampled, and root-raised cosine (RRC) shaped to generate independent LSB and RSB vector signals. Then, they modulate intermediate-frequency carriers in the form of a complex sinusoidals $\exp(j2\pi f_s t)$ and $\exp(-j2\pi f_s t)$ for generating LSB and RSB signals, respectively [26–29]. We defined the signal with a negative frequency as the LSB signal and that with a positive frequency as the RSB signal. Note that LSB and RSB signals could have identical or different baud rates and adopt identical or different modulation formats. Therefore, by means of simultaneous digital up-conversion, LSB vector signals are upconverted at negative frequencies $-f_s$, while the RSB vector signals are upconverted at positive frequencies f_s.

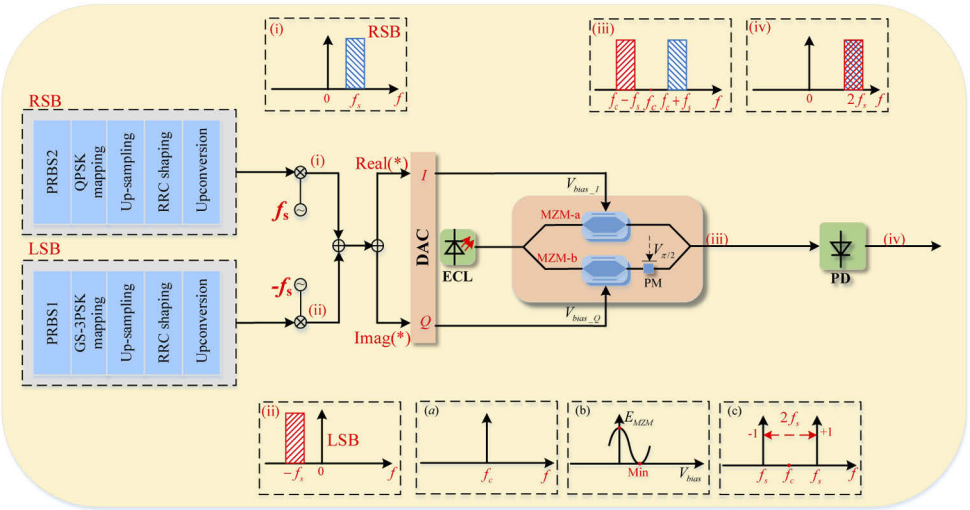

Fig. 1. LSB and RSB signal generation based on OCS and twin-SSB modulation by an I/Q modulator. PRBS: pseudo-random binary sequence; RRC: root raised cosine; ECL: external cavity laser; PM: phase modulator; MZM: Mach–Zehnder modulator; PD: photodiode. (a) Center frequency of the continuous wave produced by the ECL. (b) Relationship between output power of the MZM modulator corresponding to bias voltage. (c) Optical carrier schematic diagram after passing through the MZM modulator. (i) The schematic diagram of the RSB signal. (ii) The schematic diagram of the LSB signal. (iii) The schematic diagram the modulated signal after passing through the I/Q modulator. (iv) The schematic diagram of the received signal after the PD.

Here, the LSB and RSB carrier frequencies selected were equal. In fact, the LSB and RSB vector signal carrier frequencies can be identical or different. The LSB and RSB carrier signals can be expressed as follows:

$$E_l(t) = E_{LSB}(t)\exp(-j2\pi f_s t) \tag{1}$$

$$E_r(t) = E_{RSB}(t)\exp(j2\pi f_s t) \tag{2}$$

where $E_l(t)$ and $E_r(t)$ represent the LSB and RSB signals, respectively. Schematics of the upconverted LSB and RSB signals are illustrated in Figs. 1(ii) and (i), respectively. The two

Optics EXPRESS

sideband signals are then added and can be expressed as follows:

$$E(t) = E_l(t) + E_r(t) \tag{3}$$

As shown in Fig. 1, the real and imaginary parts of the added signal are loaded into the input ports of a DAC. Next, the electrical I-path signal and Q-path signal outputs of the DAC are used to drive the I and Q ports of an I/Q modulator, respectively [26–29]. A continuous light wave with central frequency f_c is emitted from an external cavity laser (ECL) and then injected into the I/Q modulator for the optical input port of the I/Q modulator. We adjusted the I/Q modulator in two steps. In the first step, we need to adjust the direct current (DC) bias of a single Mach-Zehnder modulator (MZM) to realize OCS modulation, and MZM-a and MZM-b are DC biased at the minimal output power point, as shown in Fig. 1(b). The second step is to adjust the phase modulator, which ensures that it has a $\pi/2$ phase shift. At the output of the I/Q modulator, the optical center carrier is mainly suppressed and two tones are generated with a channel spacing of $2f_s$, thereby realizing a frequency-doubling operation, as shown in Fig. 1(c). As shown in Fig. 1(iii), at the output of the I/Q modulator, two independent LSB and RSB vector signals are generated with frequencies $f_c - f_s$ and $f_c + f_s$, respectively. The optical signal generated from the I/Q modulator can be expressed as:

$$E_{I/Q}(t) = E_{CW}(t)[J_{-1}(\beta A_l)\exp(-j\omega_l t + j\varphi_l) + J_1(\beta A_r)\exp(j\omega_r t + j\varphi_r)] \tag{4}$$

where $J_{-1}(.)$ and $J_1(.)$ are the Bessel functions of the first class, β is the modulator modulation depth and A_l and A_r are the amplitude of the left and right sideband signals, respectively. Finally, the modulated LSB signals beat with each other and beat with other sidebands at the PD, and the received electrical vector signals are generated after the PD. A schematic is shown in Fig. 1(iv), which is a mixed signal from the LSB and RSB. The generated photocurrent is expressed as follows:

$$i_{RF}(t) = RJ_{-1}(\beta A_l)J_1(\beta A_r)\cos[(\omega_l + \omega_r)t + (\varphi_l(t) + \varphi_r(t))] \tag{5}$$

where R is the photoelectric conversion efficiency. It can be observed from Eq. (5) that the frequency of the received signal $(\omega_l + \omega_r)$ is the sum of the frequencies of the LSB and RSB signals, the phase $(\varphi_l(t) + \varphi_r(t))$ is the sum of the phases of the LSB and RSB signals, and the amplitude $J_{-1}(\beta A_l)J_1(\beta A_r)$ is the product of two Bessel functions of the first kind. The subsequent DSP algorithm is used to recover the 12QAM signal and separate the LSB and RSB signals.

2.2. Principle of separating LSB and RSB signals

It can be observed from Eq. (5) that the phase of the received electric vector signal $(\varphi_l(t) + \varphi_r(t))$ is the sum of the phases of the LSB and RSB signals $\varphi_l(t)$ and $\varphi_r(t)$, and the amplitude is related to $J_{-1}(m_l)J_1(m_r)$.

Figures 2(a)–2(c) show the constellations of the GS-3PSK, QPSK, and 12QAM vector signals detected by the PD. The LSB signal is modulated by GS-3PSK, and the initial phase is $(0, 7\pi/8, 9\pi/8)$. The RSB signal is modulated by QPSK, and the initial phase is $(\pi/4, 3\pi/4, 5\pi/4, 7\pi/4)$. According to Eq. (4), the signal phase of the received 12QAM after the PD can be expressed as follows:

$$(\pi/8, 2\pi/8, 3\pi/8, 5\pi/8, 6\pi/8, 7\pi/8, 9\pi/8, 10\pi/8, 11\pi/8, 13\pi/8, 14\pi/8, 15\pi/8)$$

Figures 2(d)–2(f) illustrate the phase relationship between the 12QAM vector signal and LSB GS-3PSK and RSB QPSK vector signals with different colors. In Fig. 2(d), yellow, cyan, and black represent different phases of the LSB GS-3PSK vector signal constellation. In Fig. 2(e), orange, green, red, and blue represent different phases of the RSB QPSK vector signal constellation. In

Optics EXPRESS

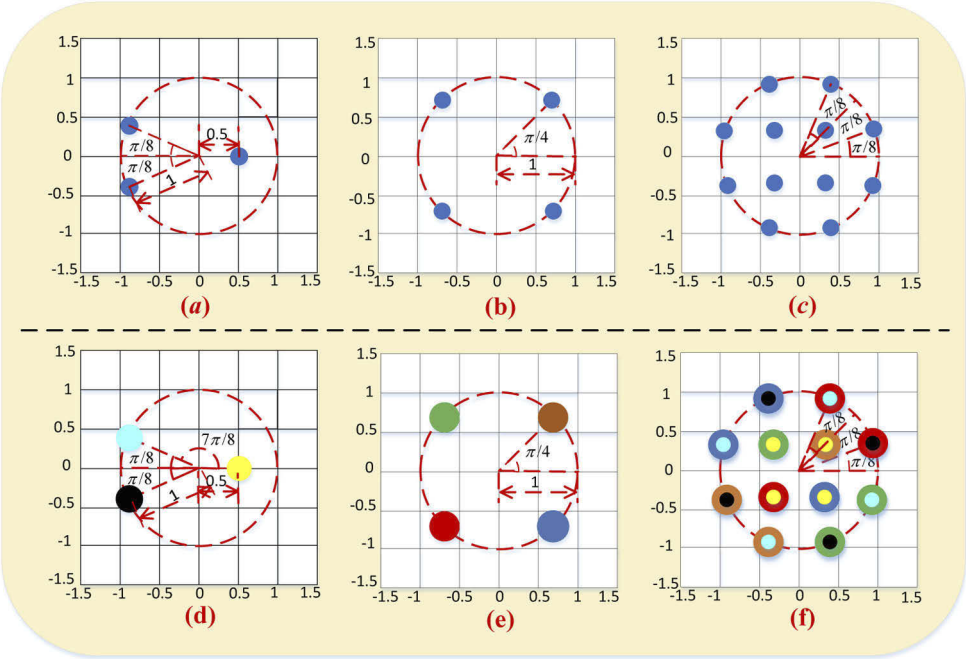

Fig. 2. Constellations of GS-3PSK, QPSK, and 12QAM vector signals. (a) Constellation of the original GS-3PSK vector signal. (b) Constellation of the original QPSK vector signal. (c) Constellation of the 12QAM vector signal after the PD. (d) Constellations of the GS-3PSK vector signal denoted by different colors. (e) Constellations of the QPSK vector signal denoted by different colors. (f) Constellations of the 12QAM vector signal denoted by different colors after the PD.

Fig. 2(f), each signal consists of two colors, which represent the GS-3PSK vector signal and QPSK vector signal beating to generate the 12QAM vector signal.

Because the color correspondence relationship reflects the mapping relationship between the received signal and the two sideband signals, the received signal can be separated at the receiver side using a simple DSP algorithm. For example, consider a constellation point with a phase of π/8. The constellation point is composed of black and red colors, which indicates that it is generated by the beating of LSB GS-3PSK black signal constellation point with phase 9π/8 and the RSB QPSK red signal constellation point with phase 5π/4. Therefore, at the received side, the phase π/8 12QAM signal is separated as phase 9π/8 GS-3PSK and phase 5π/4 QPSK signals using a simplified offline DSP algorithm. Therefore, two OBPFs and PDs are not required to separate the LSB and RSB signals. In addition, because only one mixed-signal path was sent to MATLAB for DSP, the complexity of the received-side calculation was reduced.

3. Simulation setup

Figure 3 shows the simulation setup for the novel twin-SSB scheme without OBPFs separating the two sideband signals. On the transmission side, single-drive MZM-a and MZM-b have a half-wave voltage of ~2.5 V. A continuous wave of 1548.706 nm was generated from an ECL with a linewidth of <100 kHz and an output power of 16 dBm. The offline DSP operation was implemented using MATLAB. The PRBS word length was 2^{14}. GS-3PSK modulation was adopted for the LSB vector signal (see Fig. 3(a) for the constellation diagram), while QPSK modulation was adopted for the RSB vector signal (see Fig. 3(b) for the constellation diagram).

Optics EXPRESS

The two independent sidebands have identical baud rates at 1-, 2-, 4- and 8-Gbaud. Both are linearly upconverted to the LSB vector signal located at −12-GHz and the RSB vector signal located at 12-GHz. The measured LSB and RSB spectra are shown in Figs. 3(i) and 3(ii), respectively. The I-path (the real part of $E(t)$) and Q-path (the imaginary part of $E(t)$) signals from the DAC are amplified by a pair of electronic amplifiers Then, they are simultaneously sent to the input port of the I/Q modulator. We adjusted the DC bias of the I/Q modulator to ensure that the central optical carrier has a proper power that is close to that of the LSB and RSB signals. Figure 3(iii) shows the calculated output optical spectrum of the I/Q modulator, showing two independent GS-3PSK and QPSK sidebands spaced at 12-GHz from the central optical carrier.

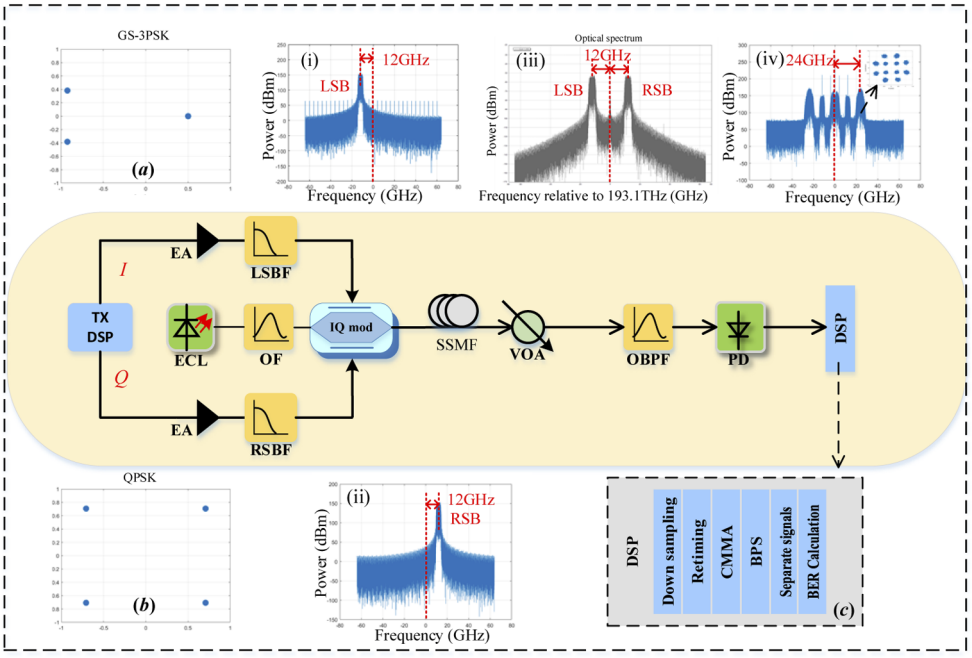

Fig. 3. Simulation setup of the novel twin-SSB system adopting OCS modulation enabled by an I/Q modulator. (a) Constellations of LSB GS-3PSK. (b) Constellations of RSB QPSK. (c) Principle of DSP at the receiver side. (i) Spectrum of the LSB GS-3PSK signal. (ii) Spectrum of the RSB QPSK signal. (iii) Optical spectra of the signal after passing through the I/Q modulator. (iv) Spectrum of the received 12QAM signal. EA: electrical amplifier; LSBF: left sideband filter; RSBF: right sideband filter, VOA: variable optical attenuator.

The generated optical signal was input into the SSMF transmission over 10-km. A variable optical attenuator (VOA) was employed before the OBPF to adjust the input power to each PD for BER measurement. We added a 30-GHz OBPF in front of the PD to limit the bandwidth of the PD. After the OBPF, the optical signals are detected by a single-ended PD, and Fig. 3(iv) shows the calculated output electrical signal spectrum of the PD. The received mixed information is recovered and separated by using an offline DSP algorithm [30–32]. This algorithm performs down-conversion to the baseband signal, performs retiming, implements a cascaded multi-modulus algorithm (CMMA) for 12QAM, conducts a blind phase search (BPS), separates mixed LSB and RSB signals, and calculates the BER [33–36]. The received-side DSP algorithm is illustrated in Fig. 3(c).

Optics EXPRESS

4. Simulation results

As shown in Figs. 3, we simulated the generation of 1-, 2-, 4-, and 8-Gbaud LSB −12-GHz GS-3PSK modulated and RSB 12-GHz QPSK modulated vector signals and SSMF back-to-back (BTB) transmission for 5- and 10-km, respectively. Figure 4 shows the received constellations of 12QAM under BTB transmission at a received optical power −8 dBm.

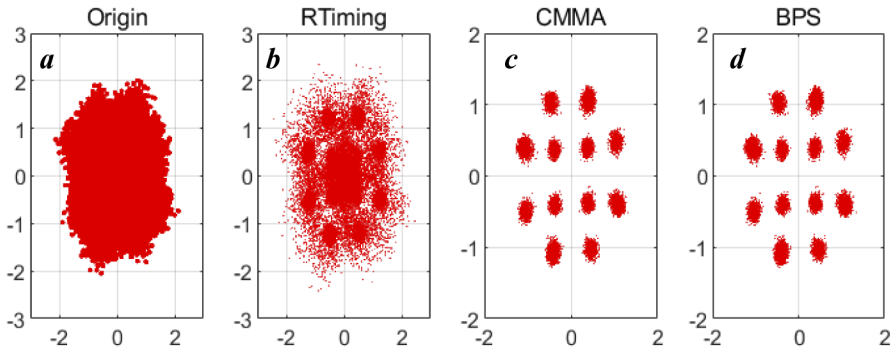

Fig. 4. Constellation of 24-GHz 4-Gbaud 12QAM vector signal under BTB transmission. (a) Constellation of received 12QAM vector signal after the PD. (b) Constellation of received 12QAM vector signal after retiming. (c) Constellation of received 12QAM vector signal after treatment by the CMMA. (d) Constellation of received 12QAM vector signal after BPS.

Figures 4(a)–4(d) correspond to the DSP procedure after the PD, after retiming, after treatment by the CMMA, and after the BPS, respectively. The LSB GS-3PSK and RSB QPSK signals can then be separated from the received 12QAM signal through a simple DSP algorithm and BER calculation.

Figure 5 shows the measured BER versus the received optical power of the PD for 1-, 2-, 4-, and 8-Gbaud LSB GS-3PSK −12-GHz and RSB QPSK 12-GHz vector signals under BTB transmission, respectively. The BERs of both the LSB GS-3PSK and RSB QPSK signals are less than the HD-FEC threshold of 3.8×10^{-3} for all the different baud rate cases. When the received optical power was >-15 dBm, almost no error was measured in all four cases. It is observed that, for the same baud rate case, two independent twin-SSB 12-GHz vector signals (corresponding to LSB and RSB, respectively) have quite similar BER performances. At the HD-FEC threshold of 3.8×10^{-3}, compared to the 1-Gbaud case, there exist 1.4, 2.7, and 4.2 dB power penalties for the 2-, 4-, and 8-Gbaud cases, respectively. The degradation of the BER performance with the increase in the baud rate is mainly due to the limited hardwares bandwidth.

In the case of the 5-km SSMF transmission, Fig. 6 shows the measured BER versus the received optical power of the PD for 1-, 2-, 4-, and 8-Gbaud −12-GHz LSB GS-3PSK and 12-GHz RSB QPSK vector signals, respectively. The BERs of both the LSB GS-3PSK and RSB QPSK signals can still reach below the HD-FEC threshold of 3.8×10^{-3} for all the different baud rate cases. Compared with BTB transmission, however, it is observed that some power penalty is caused after 5-km of SSMF transmission at the HD-FEC threshold of 3.8×10^{-3} case. For the 8-Gbaud rate case, when the received optical power is > -17 dBm, the received LSB and RSB signals can reach the original signal. BTB 8-Gbaud transmission requires a received optical power of only $>$ −16 dBm.

In the 10-km SSMF transmission case (see Fig. 7), compared with the BTB and 5-km SSMF transmission scenarios, there is an obvious degradation of BER performance. For the 4-Gbaud scenario, the receiver sensitivity loss is 2 or 3 dB at a BER of 3.8×10^{-3} after 10-km SSMF transmission. With baud rates increasing to 8-Gbaud, the LSB and RSB BER performances failed to reach the HD-FEC threshold of 3.8×10^{-3}. The serious degradation of BER performance with

Optics EXPRESS

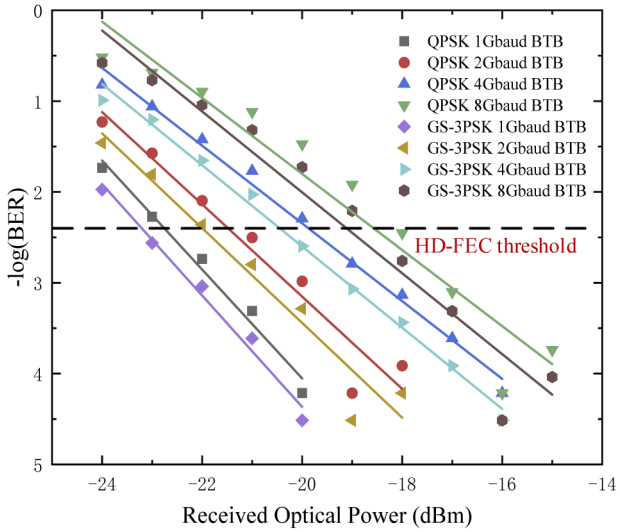

Fig. 5. BER versus received optical power with different baud rates in BTB transmission.

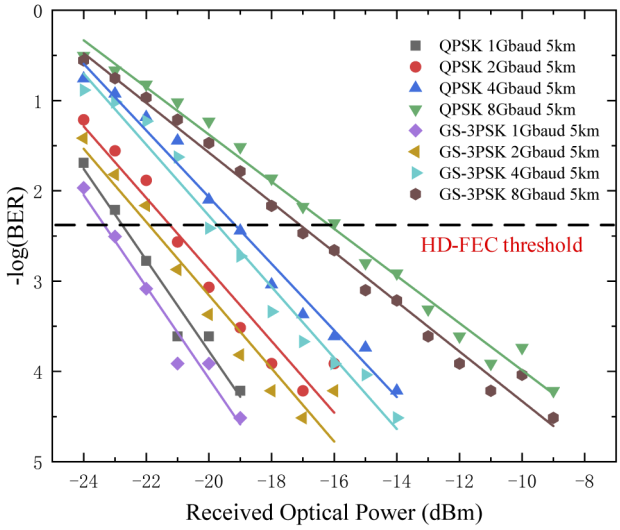

Fig. 6. BER versus received optical power with different baud rates in 5-km SSMF transmission.

an increase in the baud rate and transmission is mainly due to the limited hardwares bandwidth, which is particularly insufficient for the generation of 12-GHz sidebands carrying 8-Gbaud data transmitting over 10-km.

It is observed that, for our proposed twin-SSB system, by avoiding using OBPFs to separate the LSB and RSB signals, we can still achieve good BER performance of the two sideband signals

Optics EXPRESS

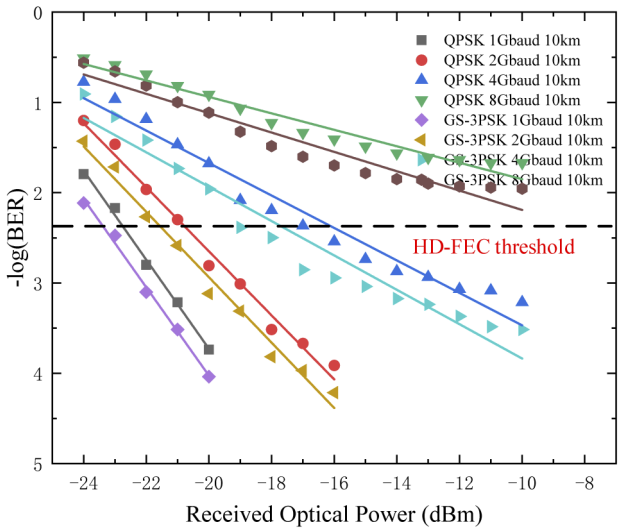

Fig. 7. BER versus received optical power with different baud rates in 10-km SSMF transmission.

5. Conclusion

The existing twin-SSB scheme includes two OBPFs and PDs to filter and detect LSB and RSB signals, which increase system complexity, system cost, and algorithm complexity. Hence, we proposed a novel twin-SSB scheme, in which no OBPFs are needed to separate two independent sideband signals and only a single-ended PD is employed for direct detection. At the receiver side, only the one-path DSP algorithm is used to recover the original signals and separate the LSB GS-3PSK and RSB QPSK vector signals. Using our scheme, we demonstrated the simultaneous generation and SSMF delivery of two independent −12-GHz LSB GS-3PSK and 12-GHz RSB QPSK vector signals, each of which can carry up to 8-Gbaud transmitter data with a BER of $<3.8 \times 10^{-3}$ over 5-km SSMF transmission and to 4-Gbaud transmitter data with a BER of $<3.8 \times 10^{-3}$ over 10-km SSMF transmission. We believe that our proposed novel twin-SSB system further reduces the complexity and cost of the system structure, which has broad application prospects for future short-distance transmission.

Funding. National Key Research and Development Program of China under contract (2018YFB1801500); National Natural Science Foundation of China (61675048); Research Project of Key Laboratory for Information Science of ElectromagneticWaves (MoE) (EMW201911).

Disclosures. The authors declare no conflicts of interest.

Data availability. Data underlying the results presented in this paper are not publicly available at this time but may be obtained from the authors upon reasonable request.

References

1. Y. Li, G. Yang, Y. Zhu, X. Ding, and X. Sun, "Unimodal stopping model-based early SKIP mode decision for high-efficiency video coding," IEEE Trans. Multimedia **19**(7), 1431–1441 (2017).
2. J. Mei, K. Li, A. Ouyang, and K. Li, "A profit maximization scheme with guaranteed quality of service in cloud computing," IEEE Trans. Comput. **64**(11), 3064–3078 (2015).
3. Y. Chen, R. Hu, Q. Yang, M. Luo, S. Yu, and W. Li, "Two orthogonal carriers assisted 101-gb/s dual-band ddo-ofdm transmission over 320-km ssmf," Opt. Express **23**(9), 12065 (2015).
4. D. Zibar, R. Sambaraju, A. Caballero, J. Herrera, U. Westergren, A. Walber, J. B. Jensen, J. Martí, and I. T. Monroy, "High-capacity wireless signal generation and demodulation in 75- to 110 GHz band employing all optical OFDM," IEEE Photonics Technol. Lett. **23**(12), 810–812 (2011).
5. X. Li, Z. Dong, J. Yu, N. Chi, Y. Shao, and G. K. Chang, "Fiber wireless transmission system of 108-Gb/s data over 80-km fiber and 2×2 MIMO wireless links at 100 GHz W-Band frequency," Opt. Lett. **37**(24), 5106–5108 (2012).

Optics EXPRESS

6. Z. Cao, J. Yu, M. Xia, Q. Tang, Y. Gao, W. Wang, and L. Chen, "Reduction of intersubcarrier interference and frequency-selective fading in OFDM-ROF systems," J. Lightwave Technol. **28**(16), 2423–2429 (2010).
7. C. Liu, H. C. Chien, S. H. Fan, J. Yu, and G. K. Chang, "Enhanced vector signal transmission over double-sideband carrier-suppressed optical millimeter-waves through a small LO feedthrough," IEEE Photonics Technol. Lett. **24**(3), 173–175 (2012).
8. X. Li, J. Yu, J. Zhang, Z. Dong, F. Li, and N. Chi, "A 400G optical wireless integration delivery system," Opt. Express **21**(16), 18812–18819 (2013).
9. J. Yu, X. Li, and N. Chi, "Faster than fiber: over 100-Gb/s signal delivery in fiber wireless integration system," Opt. Express **21**(19), 22885–22904 (2013).
10. I. S. Amiri, E. S. Alavi, and M. S. Idrus, "W-Band OFDM transmission for radio-over-fiber link using solitonic millimeter wave generated by MRR," IEEE J. Quantum Electron. **50**(8), 622–628 (2014).
11. T. Cho and K. Kim, "Effect of third-order intermodulation on radio-over-fiber systems by a dual-electrode Mach-Zehnder modulator with ODSB and OSSB signals," J. Lightwave Technol. **24**(5), 2052–2058 (2006).
12. V. Sharma and S. Kumar, "Hybrid OFDM-OSSB-RoF transmission system incorporating fiber Bragg grating," Optik **124**(20), 4670–4672 (2013).
13. Y. Wang, J. Yu, H. C. Chien, X. Li, and N. Chi, "Transmission and direct detection of 300-Gbps DFT-S OFDM signals based on O-ISB modulation with joint image-cancellation and nonlinearity-mitigation," Opt. Commun. 1–3 (2016).
14. H. C. Chien, Z. Jia, J. Zhang, Z. Dong, and J. Yu, "Optical independent sideband modulation for bandwidth-economic coherent transmission," Opt. Express **22**(8), 9465–9470 (2014).
15. Y. Zhu, X. Ruan, K. Zou, and F. Zhang, "Beyond 200G direct detection transmission with Nyquist asymmetric twin-SSB signal at C-band," J. Lightwave. Technol. **35**(17), 3629–3636 (2017).
16. M. Chen, M. Peng, H. Zhou, Z. Zheng, X. Tang, and L. Maivan, "Receiver sensitivity improvement in spectrally-efficient guard-band twin-SSB-OFDM using an optical IQ modulator," Opt. Commun. **405**, 259–264 (2017).
17. X. Chen, C. Antonelli, A. Mecozzi, D. Che, and W. Shieh, "High-capacity direct-detection systems," in *Optical Fiber Telecommunications VII*, 419–441 (2020).
18. J. Li, F. Zhao, and J. Yu, "D-band vector signal generation based on OCS and SSB without an optical filter," Opt. Commun. **464**, 125520 (2020).
19. Z. Dong, H. C. Chien, J. Yu, J. Zhang, L. Cheng, and G. Chang, "Very high-throughput coherent ultra-dense WDM-PON based on Nyquist-ISB modulation," IEEE Photonics Technol. Lett. **27**(7), 763–766 (2015).
20. L. Zhang, T. Zuo, Q. Zhang, J. Zhou, E. Zhou, and G. N. Liu, "150-Gb/s DMT over 80-km SMF transmission based on spectrally efficient SSBI cancellation using guard-band twin-SSB technique," Opt. Commun. 1178–1180 (2016).
21. L. Zhang, T. Zuo, Q. Zhang, J. Zhou, E. Zhou, and G. N. Liu, "Single wavelength 248-Gb/s transmission over 80-km SMF based on twin-SSB DMT and direct detection," Opt. Commun. Dusseldorf, Germany, 133–135 (2016).
22. L. Zhang, T. Zuo, Q. Zhang, E. Zhou, G. N. Liu, and X. Xu, "Transmission of 112-Gb/s DMT over 80-km SMF by Twin-SSB Technique," Opt. Commun. **0373**, 1–3 (2015).
23. M. Zhu, L. Zhang, J. Wang, L. Chen, C. Liu, and G.-K. Chang, "Radioover-fiber access architecture for integrated broadband wireless services," J. Lightwave Technol. **31**(23), 3614–3620 (2013).
24. R. Deng, J. Yu, and J. he, "Twin-SSB-OFDM transmission over heterodyne W-band fiber-wireless system with real-time implementable blind carrier recovery," J. Lightwave Technol. **36**(23), 5562–5572 (2018).
25. X. Gao, Y. Cai, B. Xu, F. K. Deynu, and K. Qiu, "Zero Guard Band Multi-Twin-SSB System in Single Fiber Bidirectional PON Transmission," IEEE Access, p.26814 (2020).
26. Z. Xu, R. Hui, and M. O'Sullivan, "Dual-band OOFDM system based on tandem single-sideband modulation transmitter," Opt. Express **17**(16), 13479–13486 (2009).
27. L. Zhang, Q. Zhang, T. Zuo, E. Zhou, G. N. Liu, and X. Xu, "C-band single wavelength 100-Gb/s IM-DD transmission over 80-km SMF without CD compensation using SSB-DMT," *Opt. Fiber Commun. Conf.* (2015).
28. X. Pan, B. Zhang, and X. Liu, "Mitigation of crosstalk between RSB and LSB signals generated by one I/Q modulator," Opt. Express **28**(2), 2238–2250 (2020).
29. X. Pan, X. Liu, H. Zhang, K. Wang, Y. Zhang, D. Ran, X. Wang, and C. Wang, "Independent dual single-sideband vector millimeter-wave signal generation by one single I/Q modulator," Opt. Express **27**(14), 19906–19914 (2019).
30. X. Li, J. Yu, J. Xiao, and Y. Xu, "Fiber-wireless-fiber link for 128-Gb/s PDM-16QAM signal transmission at W-band," IEEE Photonics Technol. Lett. **26**(19), 1948–1951 (2014).
31. L. Zhao, J. Yu, L. Chen, P. Min, J. Li, and R. Wang, "16QAM vector mm-wave signal generation based on phase modulator with photonic frequency doubling and pre-coding," IEEE Photonics J. **8**(2), 1–8 (2016).
32. J. Zhang, Z. Dong, J. Yu, N. Chi, L. Tao, X. Li, and Y. Shao, "Simplified coherent receiver with heterodyne detection of eight-channel 50 Gb/s PDM-QPSK WDM signal after 1040 km SMF-28 transmission," Opt. Lett. **37**(19), 4050–4052 (2012).
33. X. Li, J. Xiao, and J. Yu, "Long-Distance Wireless mm-Wave Signal Delivery at W-Band," J. Lightwave Technol. **34**(2), 661–668 (2016).
34. J. Yu and X. Zhou, "Ultra-high-capacity DWDM transmission system for 100G and beyond," IEEE Commun. Mag. **48**(3), S56–S64 (2010).
35. J. Yu, X. Li, and W. Zhou, "Tutorial: Broadband fiber-wireless integration for 5G+ communication," APL Photonics **3**(11), 111101 (2018).
36. J. Yu, "Photonics-Assisted Millimeter-Wave Wireless Communication," IEEE J. Quantum Electron. **53**(6), 1–17 (2017).